


# Robust and Antibacterial Polymer/Mechanically Exfoliated Graphene Nanocomposite Fibers for Biomedical Applications

Yu Ma,<sup>†,‡</sup> Dongchen Bai,<sup>§</sup> Xinjun Hu,<sup>†</sup> Nan Ren,<sup>†</sup> Wensheng Gao,<sup>†</sup> Songbo Chen,<sup>†</sup> Huqiang Chen,<sup>†</sup> Yue Lu,<sup>†</sup> Jiangong Li,<sup>†</sup> and Yongxiao Bai<sup>\*,†</sup> 

<sup>†</sup>Institute of Material Science and Engineering, Key Laboratory for Magnetism and Magnetic Materials of the Ministry of Education, Key Laboratory of Special Function Materials and Structure Design of Ministry of Education, Lanzhou University, Lanzhou 730000, China

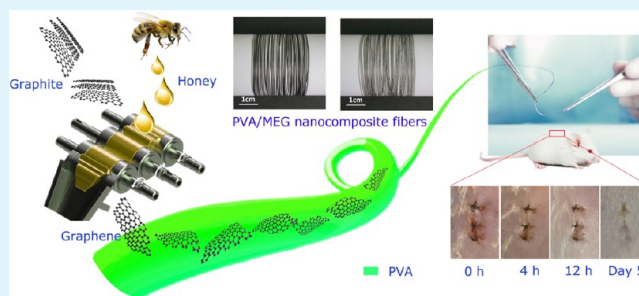
<sup>‡</sup>Department of Chemical Engineering and Biointerfaces Institute, University of Michigan, Ann Arbor, Michigan 48109-2136, United States

<sup>§</sup>No. 1 Middle School of Lanzhou, Lanzhou 730000, China

## Supporting Information

**ABSTRACT:** With the increasing demand for composites of multifunctional and integrated performance, graphene-based nanocomposites have been attracting increasing attention in biomedical applications because of their outstanding physicochemical properties and biocompatibility. High product yields and dispersion of graphene in the preparation process of graphene-based nanocomposites have long been a challenge. Further, the mechanical properties and biosafety of final nanocomposites are very important for real usage in biomedical applications. Here, we presented a novel high-throughput method of graphene on mechanical exfoliation in a natural honey medium, and a yield of ~91% of graphene nanoflakes can be easily achieved with 97.76% of single-layer graphenes. The mechanically exfoliated graphene (MEG) can be well-dispersed in the poly(vinyl alcohol) (PVA) matrix. The PVA/MEG nanocomposite fibers are obtained by gel spinning and stretched 20 times. As a candidate for monofilament sutures, the PVA/MEG nanocomposite fibers with 0.3 wt % of MEG have an ultrahigh ultimate tensile strength of 2.1 GPa, which is far higher than that of the neat PVA fiber (0.75 GPa). In addition, the PVA/MEG nanocomposite fibers also have antibacterial property, low cytotoxicity, and other properties. On the basis of the above-mentioned properties, the effects of a common surgical suture and PVA/MEG nanocomposite fibers on wound healing are evaluated. As a result, the wounds treated with PVA/MEG nanocomposite fibers with 0.3 wt % of MEG show the best healing after 5 days of surgery. It is possible that this novel surgical suture will be available in the market relying on the gentle, inexpensive method of obtaining nonoxidized graphene and the simple process of obtaining nanocomposite fibers.

**KEYWORDS:** *graphene, nanocomposite fibers, mechanical exfoliation, surgical suture, biocompatible*



## 1. INTRODUCTION

Over the past decade, polymer-based nanocomposites have generated great interest because of their wide applications in the fields of energy technology,<sup>1</sup> environmental treatment,<sup>2</sup> and biomedical.<sup>3</sup> As a water-soluble and biocompatible polymer, poly(vinyl alcohol) (PVA) can be used as a biomedical material,<sup>4</sup> such as skin suture, but much better mechanical properties and more functions are needed. Until now, a few attempts have been made to enhance the PVA fibers with a variety of nanofillers. Among these nanofillers, carbon-based materials have been exploited for their excellent mechanical and electrical properties. Multiwalled carbon nanotubes (MWCNTs)<sup>5</sup> and single-walled carbon nanotubes (SWCNTs)<sup>6</sup> have been used in the PVA matrix, but their impacts of enhancement on the mechanical properties still have a potential for improvement. Besides these carbon materials, graphene has

attracted more attention because of its outstanding physical,<sup>7</sup> antibacterial,<sup>8</sup> and other properties.<sup>9</sup> The combination of graphene and PVA may improve the tensile strength of the fiber because the two-dimensional (2D) structure of graphene helps to transfer the force between the ends of the polymer or to give the nanocomposite fiber some new functionality. However, the preparation of PVA/graphene nanocomposite fibers that can be commercially used in the biomedical field is still handicapped by the following problems: (1) the good dispersion of graphene in PVA; (2) graphene must be cheap and widely available and the preparation of nanocomposite fibers should be as simple as possible for market development

**Received:** November 23, 2017

**Accepted:** January 2, 2018

**Published:** January 2, 2018

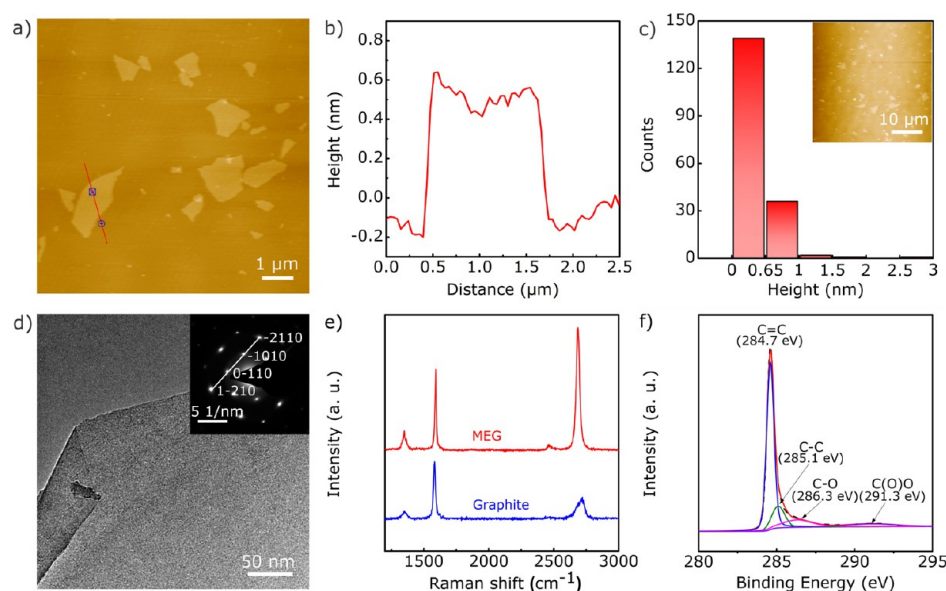


**Figure 1.** Characterization of MEG flakes. (a) AFM image of a monolayer graphene sheet and (b) corresponding height profile. (c) Statistical thickness analysis of 179 MEG flakes in the inset AFM image. (d) TEM image of the monolayer graphene and SAED pattern (inset) from the flake. (e) Raman spectra of natural graphite and MEG. (f) XPS of the C 1s signal of MEG.

in this area; and (3) to be used for biomedical applications, composite fibers must be safe for humans.

To overcome these problems, various efforts have been tested in recent years. Wang et al. prepared graphene oxide (GO)/PVA composite nanofibers via electrospinning, but they are not practical because of the small diameter of 0.5  $\mu\text{m}$  and the low tensile strength of 16 MPa.<sup>10</sup> Li et al. reported that the PVA/reduced GO (rGO) composite fibers were prepared by wet spinning, and the tensile strength of the 2.0 wt % rGO and PVA composite fiber is 867 MPa.<sup>11</sup> Obviously, a large amount of graphene consumed and the low tensile strength suggest that this method is still not as adequate as an ideal solution. Li et al. and Hu et al. also prepared PVA/rGO composite fibers, and the tensile strength of the composite fibers was increased.<sup>12,13</sup> However, none of these strategies satisfactorily solved the aforementioned problems. Although the oxygenated groups of rGO can hydrogen bond with the  $-\text{OH}$  groups of PVA, which will contribute to enhancing the mechanical properties, preparation of GO by the Hummers' method relies on strong acids and strong oxidants. Efforts to treat the wastewater environmentally are costly.<sup>14,15</sup> More importantly, it has the risk of causing oxidative stress in human cells for biomedical applications.<sup>16</sup> It was reported that the interaction of the surfaces of GO and rGO with the antioxidant glutathione and oxygen groups show a strong catalytic activity. Therefore, it may thereby mediate oxidative damage in living systems. However, it is also a problem if graphene has no oxidized groups and whether it will have a strong effect with PVA. In fact, graphene will be closely bonded with PVA to reduce its surface energy.

On the other hand, PVA/graphene nanocomposite fibers used as surgical sutures require not only good mechanical properties but also the ability to keep bacteria away from the surgical site. This is also what the medical area is trying to solve. After all, surgical sutures are one of the most widely used medical devices nowadays. As far as we know, there are generally two types of methods for preparing antibacterial surgical sutures: "offline" and "online" processes. In the

"offline" process, the sutures are coated with a drug or soaked in the drug solution, whereas in the "online" process, the drug is added during the preparation of sutures. The difficulty of both the methods lies in how to control the release of drugs. If the release of the drug on the surface of the suture is too fast, it cannot play a role in the entire period of trauma recovery. The drug in the suture is often difficult to be released because of its conjugation with polymers. It should be noted that graphene has been tested to have a good antibacterial effect and that its sharp edges can cause physical damage to nearby bacteria. This may be a new way to solve the antibacterial problem of the surgical line. Therefore, it strongly desires to design an unoxidized graphene and PVA nanocomposite fibers with good mechanical and antibacterial properties. Crucially, graphene, as a filler, should be obtained by a nonoxidizing, low-cost, high-yield method, and the process of producing the nanocomposite fibers should be as simple as possible for commercial production.

In this study, we report a green, simple, low-cost method for preparing high-quality graphene with a high yield of  $\sim 91\%$  on a three-roll mill by using natural honey as exfoliating media. Then, a series of PVA/mechanically exfoliated graphene (MEG) nanocomposite fibers were prepared by gel spinning. The ultimate tensile strength of PVA/MEG nanocomposite fibers is 2.1 GPa, which increased 180% over the pure PVA fibers, showing a huge potential for skin suturing. In the meantime, the antibacterial property and cytotoxicity of PVA/MEG nanocomposite fibers were also examined. Furthermore, the PVA/MEG nanocomposite fibers, neat PVA fibers, and common surgical sutures were evaluated for a skin wound in a mice model. The result indicated that the PVA/MEG nanocomposite fiber with 0.3 wt % of MEG has better effects on the healing of the wound compared with the others. We expect these findings to be applied to other water-soluble polymers and to be applied to biomedical, tissue engineering, and other fields.

## 2. RESULTS AND DISCUSSION

**2.1. Preparation of MEG.** During the exfoliation of graphite, the viscous medium passes the energy from the three-roll mill to graphite in the form of exfoliation, which obtains mono- and few layers of graphene because of the sliding between the layers of the graphite. This means that an effective exfoliation can only occur if the surface energy of the solvent is close to that of graphite and the net energetic consumption is very small. This energy balance can be approximately calculated by the Hildebrand–Scatchard eq 1, where  $\delta_i = \sqrt{E_{\text{sur}}^i}$  is the square root of the surface energy of phase  $i$ ,  $T_{\text{MEG}}$  is the thickness of the MEG, and  $\phi$  is the volume fraction of graphene.<sup>17</sup> Because graphite has a surface energy similar to that of carbon nanotubes, Jonathan showed the maximum dispersible concentration of rigid rods in solvents (2), where  $K'$  is a constant and  $\bar{v}$  is the molar volume of rods.<sup>18</sup>

$$\frac{\Delta H_{\text{mix}}}{V_{\text{mix}}} \approx \frac{2}{T_{\text{MEG}}} (\delta_{\text{G}} - \delta_{\text{sol}})^2 \times \phi \quad (1)$$

$$\phi \approx K' \exp \left[ \frac{\bar{v}}{RT} \frac{\partial(\Delta H_{\text{mix}}/V)}{\partial \phi} \right] \quad (2)$$

We assume that the concentration of MEG ( $C_{\text{G}} \propto \phi_{\text{G}}$ ) can be described by

$$C_{\text{G}} \propto \exp \left[ \frac{\pi D_{\text{G}}^2}{8 \delta_{\text{sol}}^2 kT} (\delta_{\text{G}}^2 - \delta_{\text{sol}}^2)^2 \right] \quad (3)$$

where  $D_{\text{G}}$  is the diameter of a MEG flake. Here, the approximation  $(x - a)^2 \approx 4a(\sqrt{x} - \sqrt{a})^2$  was used. It is reasonably accurate so long as the full width at half-maximum of the resulting Gaussian is less than about half the center value. This model is consistent with the actual measured data,<sup>19</sup> suggesting a surface energy of graphene of  $\sim 68$  mJ/m<sup>2</sup>. In this case, *N*-methyl-2-pyrrolidone, dimethyl sulfoxide (DMSO), and *N,N*-dimethylformamide have been used to exfoliate graphite by different approaches. In addition to the organic and inorganic solvents discussed above, honey, a kind of green food with high stability, is another promising candidate. Most importantly, not only the surface energy and tension of honey can closely match with those of graphite, but also its viscosity on the direct stripping of graphite plays a positive role. This may be the fundamental cause of the ultrahigh yield of honey-assisted exfoliation of graphite.

After the exfoliation for 5 h, the high quality of graphene was successfully obtained from the exfoliation by the three-roll mill because of the high viscosity of honey and the layered structure of graphite. Figure 1a shows a typical atomic force microscopy (AFM) image of MEG. The thickness and diameter of the MEG are 0.65 nm and  $\sim 1$   $\mu\text{m}$ , respectively (Figure 1b). Considering the gap between the graphene flake and the mica as a substrate and the folds of the graphene flake, the height of graphene is often found to be higher than the theoretical value of 0.34 nm. When the thickness of large graphene is less than 0.65 nm, we think it as a single layer, which can be confirmed by transmission electron microscopy (TEM). In Figure 1c, the thickness analysis for the MEG in the inset AFM image shows that all of the MEG has a thickness lower than 1 nm and more than 97.76% of the sheets are thinner than 1 nm. Figure 1d shows the TEM image of a MEG, indicating that the film is very lithe and slightly curly, and the corresponding selected area electron diffraction (SAED) pattern indicates a typical

hexagonally arranged lattice of graphene. The intensities of inner 0110- and  $\bar{1}010$ -type reflections are much stronger than those of outer  $1\bar{2}10$ - and  $2\bar{1}10$ -type reflections, suggesting the identity of the monolayer graphene.<sup>20</sup>

Raman spectroscopy is performed to further study the quality and defect content of the MEG. For comparison, Raman spectra of starting graphite and MEG are shown in Figure 1e. There are three pronounced peaks used for analysis: 1346 cm<sup>-1</sup> (D band), 1575 cm<sup>-1</sup> (G band), and a second-order Raman peak (2D band) for each sample. The defect content is defined as the intensity ratio of the D band to the G band, commonly known as  $I_{\text{D}}/I_{\text{G}}$ . It is found from Figure 1e that  $I_{\text{D}}/I_{\text{G}}$  slightly increases from 0.22 for graphite to 0.27 for MEG, which is much better than that of the rGO (0.9–1.4),<sup>21</sup> indicating that few additional defects have been introduced to the edge of MEG after exfoliation for 5 h. Moreover, the number of graphene layers directly affects the position, intensity, and shape of the 2D band. The red shift and the perfect single Lorenz type have proved the presence of monolayer graphene.<sup>22,23</sup> Also, the intensity of the 2D band is stronger than that of the G band, which is the key to determine the monolayer graphene.<sup>24</sup> Figure 1f displays the X-ray photoelectron spectroscopy (XPS) spectra of the MEG, which shows a predominate C=C band at 284.7 eV. The weak signals for the C–C band (285.1 eV), C–O band (286.3 eV), and C(O)O band (291.3 eV) confirm the low content of defects in the MEG sample. In reality, natural graphite is not composed solely of carbon but also contains impurities, such as oxygen.<sup>25</sup> For comparison, we also tested the content ratio of carbon and oxygen atoms in natural graphite and graphene by XPS, and the result was 70, demonstrating that the oxygen atoms were not introduced in the milling process. To explore the quality of the MEG in an intuitive way, the electrical conductivity of the MEG film which was prepared by the vacuum filtration method was measured by using the four-point probe technique. The conductivity of the MEG film was measured to be 52 400 S/m because of less defects, which is higher than that of the graphene film prepared by the rGO.<sup>26</sup>

Figure 2a–c shows the AFM images of the graphene that was obtained at different times during the exfoliation process, and Figure 2d is a graph of the relationship between the thickness of graphene with the time of milling. As the exfoliation process was carried out further, the graphite gradually became thinner, and the monolayer graphene was obtained finally as shown in Figure 1a. This discovery may contribute to some applications that have a specific demand for the thickness of graphene.

From the above-mentioned facts, high-quality monolayer graphene and controllable layers of graphene can be easily obtained through a green approach with a very high degree of mechanization. In fact, in addition to the preparation through an environmentally friendly process, the yield is another important factor restricting industrial production. The comparison in Table 1 shows that the yields of nonoxidized graphene by similar methods are lower than our result. It is worth noting that the production by this method will dramatically increase with the effective area of a single roll or a number of rolls, exhibiting a broad prospect for industrial applications in nanocomposites and other fields.

**2.2. PVA/MEG Nanocomposite Fibers for Surgical Suture.** High-quality graphene prepared by the method we proposed is the ideal candidate of nanofillers in the matrix of PVA for monofilament sutures. The MEG with a sheet structure and large specific surface area is contributed to the

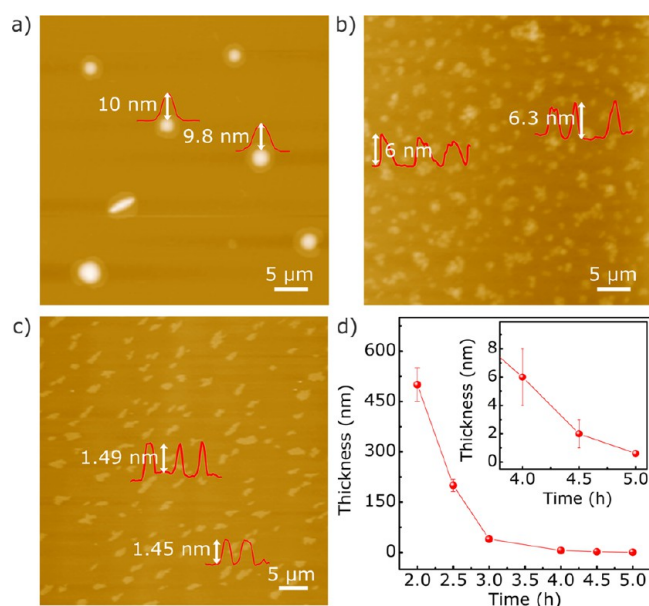


**Figure 2.** AFM analysis of the graphene materials at different periods of exfoliation. (a–c) AFM images of MEG obtained at different exfoliation times. (a) 3, (b) 4, (c) 4.5 h, and (d) correlation between the thickness of MEG and exfoliation time. The inset in (d) shows times from 4 to 5 h.

**Table 1. Comparison of the Graphene Yield Using Various Exfoliation Production Methods**

precursors	processing features	yield efficiency (%)	references
graphite	shear exfoliation	3.0	27
graphite	in $(\text{NH}_4)_2\text{CO}_3$	7–65	28
graphite	460 h bath sonication	36.4	29
graphite	1 h shear mixer	0.2	30
pyrolytic graphite	hydrothermal	~35	31
unmodified isostatic graphite	1 h stirred media milling	4.3	32
graphite	30 h ball milling	35.6	33
raw pyrolytic graphite	4–10 h hydrothermal	10	18
graphite	5 h three-roll mill	91.32	this work

stress transferring of the material, which is helpful to improve the mechanical properties of the fibers. Therefore, it is a very promising composite reinforcement. A series of different contents of MEG of nanocomposite fibers with a diameter of  $\sim 200 \mu\text{m}$  were prepared. Figure 3 shows the photographs of PVA/MEG nanocomposite fibers by the addition of different contents of MEG.

**2.2.1. Mechanical Properties of PVA/MEG Nanocomposite Fibers.** The ultimate tensile strength of the PVA/MEG nanocomposite fibers with different contents of MEG is presented in Figure 4a. The tensile strength of the nanocomposite fibers increased with the incorporation of MEG, from 751.34 MPa for neat PVA to 2102.12 MPa for the PVA/MEG nanocomposite fibers with the content of MEG at 0.3 wt %. However, with the increasing MEG, the tensile strength decreased around 1053.73 MPa with the content of 0.7 wt %. Nevertheless, the growth rate of ultimate tensile strength for PVA in this work is still higher than those in the previous reports of enhancements by other carbon materials for PVA

fibers, including MWCNT,<sup>5</sup> SWCNT,<sup>6,34</sup> and rGO<sup>12,13</sup> (see Figure 4b).

In fact, the ultimate tensile strength of the nanocomposite fibers is expected to be significantly enhanced by the good dispersion of the MEG in PVA. This can be explained from the schematic model in Figure 4c. It is assumed that there are three dispersed states of MEG in the nanocomposite fibers: (1) the MEG is dispersed in the PVA substrate independently. (2) The MEG joins together side by side in the nanocomposite fibers and transfers the strain that the nanocomposite fibers take. (3) The MEG forms blocks because it stacks together. Undoubtedly, the second situation is the ideal state, exhibiting the ultimate contribution of MEG to the tensile strength with the greatest efficiency. To investigate the dispersion state of the graphene in the nanocomposite fibers, the cross sections of the fibers were examined by a scanning electron microscopy (SEM) instrument (Figure 5). With the increase of the content of MEG, the cross sections of the fiber became rough (Figure 5a–f). The content of MEG in Figure 5c is 0.3 wt %, which is the turning point from smooth to rough. Higher than this content, the dispersion of MEG in PVA was reduced, and the MEG nanosheets were agglomerated into thick graphene sheets, weakening the efficiency of the tensile strength. The surfaces of the fibers also showed same characteristics (Figure S1). On the other hand, breakage elongations of nanocomposite fibers had the opposite trend. With the loading of MEG increasing to 0.3 wt %, the breakage elongations decreased to 13.96%. As more graphene was added, the elongation at break gradually increased to 17.92%. The close interaction between graphene and the matrix affects the movement of the polymer chains. This result shows that the MEG can effectively enhance PVA within a reasonable range of addition and the PVA/MEG nanocomposite fibers have sufficient mechanical properties as candidates for surgical sutures.

**2.2.2. Antibacterial Properties and Cytotoxicity of PVA/MEG Nanocomposite Fibers.** The ideal surgical suture should have good mechanical properties not only to provide adequate support for the tissue edge but also to prevent the breeding of bacteria. To detect the antibacterial properties of nanocomposite fibers, both Gram-positive and Gram-negative microorganisms were measured by using a viable cell-counting method. It can be seen from Figure 6a,b that fibers show the different antimicrobial effect after 4 h of exposure. The growth curves of the bacteria in contact with different fibers are shown in Figure 6c,d. It can be seen that the PVA fiber has no antimicrobial properties, and with the increase in the content of MEG, fibers showed a higher antibacterial effect. It is noteworthy that the Gram-positive bacteria are more sensitive to nanocomposite fibers than the Gram-negative bacteria. Carpio et al. also observed the same phenomenon in previous studies.<sup>35</sup> They believe that the reason why the Gram-positive bacteria are more sensitive than the negative bacteria is due to their lack of external cell membrane. They also believe that oxidative stress is one of the main mechanisms of the antibacterial behavior. However, the MEG is prepared by the mechanical method, which almost does not contain oxygen groups. The possible mechanism of the antimicrobial behavior can be explained by physical damage.<sup>36</sup> The sharp edges of the graphene flakes on the nanocomposite material can damage the cell membrane, causing the cell membrane to fall off.<sup>37</sup> Compared with oxidative stress which is caused by the rGO, the physical damage will not affect large areas of cells but only kill the adjacent bacteria.

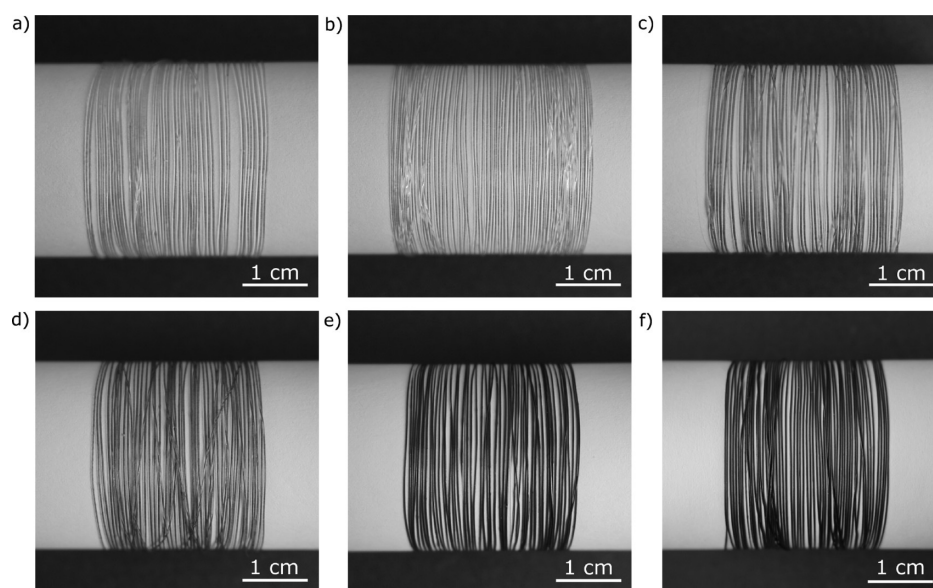


**Figure 3.** Images of PVA/MEG nanocomposite fibers with different loadings of MEG. (a) 0, (b) 0.05, (c) 0.1, (d) 0.3, (e) 0.5, and (f) 0.7 wt %.

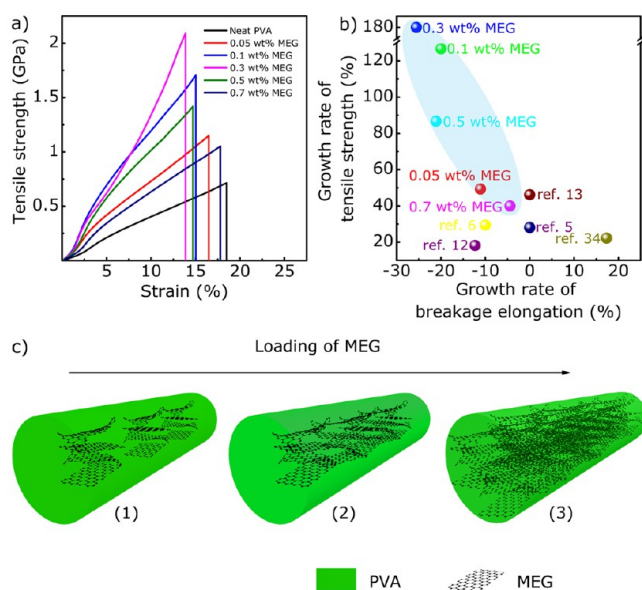


**Figure 4.** Mechanical properties of PVA/MEG nanocomposite fibers and schematic models. (a) Tensile strength of PVA/MEG nanocomposite fibers, (b) diagram of mechanical performance for PVA/carbon materials in previous and in this work (dots in the light blue area), and (c) schematic models for the dispersed states of MEG in the PVA/MEG nanocomposite fibers.

The enhanced mechanical properties of PVA fibers by MEG as well as the antibacterial properties of nanocomposite fibers show great potential, which can be used as skin suture and for tissue engineering. However, as surgical sutures, the nanocomposite fibers will come in direct contact with human tissues, so it is particularly necessary to ensure the safety of PVA/MEG nanocomposite fibers for human cells. In this work, peripheral blood mononuclear cells (PBMCs) were used to assess the cytotoxicity of PVA/MEG nanocomposite fibers with different contents of MEG. It is well-known that this cell is sensitive to exogenous toxicity. As shown in Figure 6e, after 48 h of exposure, the cells in neat PVA fiber and PVA/MEG nanocomposites with 0.05, 0.1, 0.3, and 0.5 wt % of MEG

did not show significant apoptosis, so these nanocomposite fibers have no adverse effect on these cells. However, the cells exposed to nanocomposite fibers containing 0.7 wt % of MEG were slightly reduced. According to the results, nanocomposite fibers in a certain content range of MEG are safe for PBMCs. Therefore, PVA/MEG nanocomposite fibers can be directly applied to human tissues in the current research process. However, the reason that PVA/MEG nanocomposite fibers showed opposite results to bacteria and that human cells may be related to the different size and structure of the two kinds of cells is worthy to be further explored.

In addition, other properties of nanocomposite fibers were valued, for instance, the thermal stability (Figure S2) and UV blocking (Figure S3).

**2.2.3. Wound Healing Test.** On the basis of the study of mechanical properties, antibacterial properties, and the cytotoxicity to human cells of PVA/MEG nanocomposite fibers, we selected the common surgical suture, neat PVA fiber, and three kinds of PVA/MEG nanocomposite fibers to suture mouse wounds. Figure 7a,b shows the representative images of stitched wound and unhealed wound rates during 5 post-operative days. The scalpel exposed to air for 24 h was used to cut a wound on the back of every mouse, and all the wounds were not disinfected. Then we sewed these wounds with five kinds of lines, and the ordinary interrupted suture was used. At 4 h, the wounds stitched by the common surgical suture, neat PVA fiber, and PVA/MEG nanocomposite fibers (containing 0.05 and 0.1 wt % MEG) were all inflamed by a bacterial infection. It should be noted that the common surgical suture-treated wound has severe edema with exudate, and the involution of neat PVA fiber-treated wound was not good. On the other hand, PVA/MEG nanocomposite fibers with 0.05 and 0.1 wt % MEG-treated wounds showed a certain inflammation, but the involution of wounds was good with no exudate. With further increasing the MEG content to 0.3 wt %, the nanocomposite fiber-treated groups exhibit a reduced unhealed wound area without inflammation and exudate. On the fifth day, except the common surgical suture-treated group, neat PVA fiber, and the nanocomposite fiber with 0.05 wt % of MEG-treated groups, all of the other groups have reached the

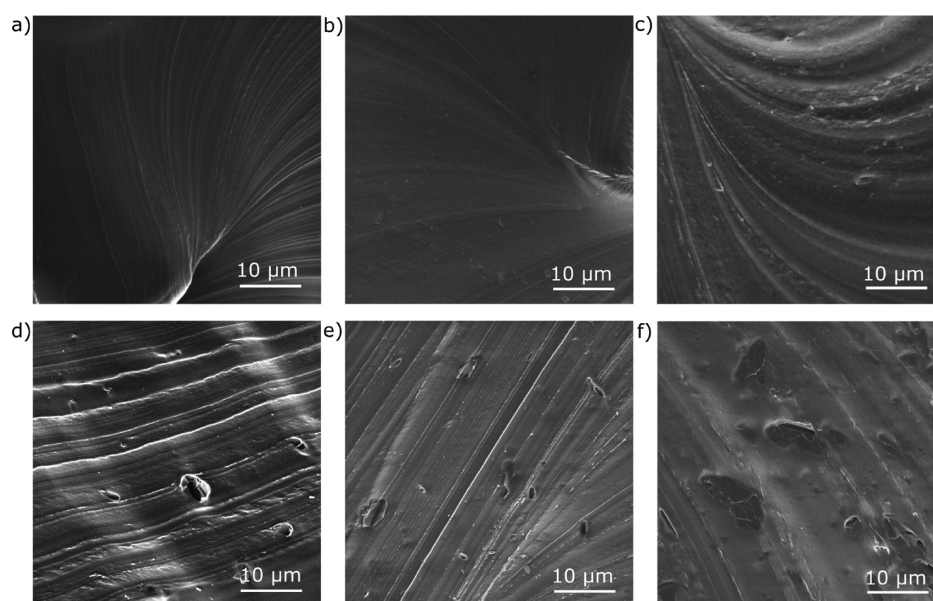


**Figure 5.** SEM images of cross sections of PVA/MEG nanocomposite fibers. (a–f) Cross sections of PVA/MEG nanocomposite fibers with loadings of 0, 0.05, 0.1, 0.3, 0.5, and 0.7% MEG, respectively.

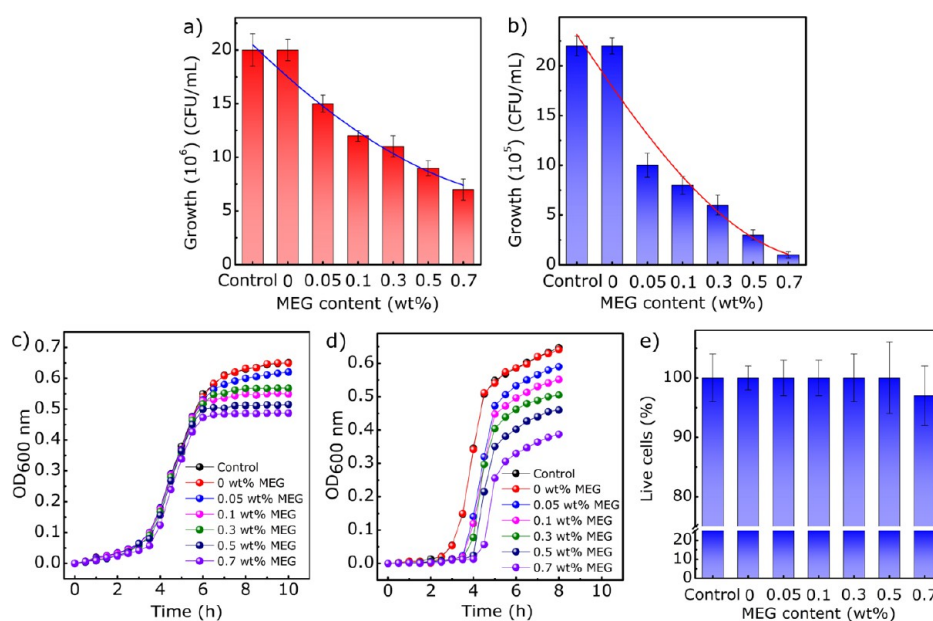


**Figure 6.** Antimicrobial activity of PVA/MEG nanocomposite fibers. Plate count result of (a) *Escherichia coli* and (b) *Staphylococcus aureus* after 4 h of exposure to PVA/MEG nanocomposite fibers with different contents of MEG; the optical measurements of (c) *E. coli* and (d) *S. aureus* under optical density (OD<sub>600</sub>) in tryptic soy broth after 4 h and exposure to each fiber, and (e) percent cytotoxicity of cells after 48 h of exposure to PVA/MEG nanocomposite fibers.

standard of the stitches that the collagen fibers on both sides of the wounds were connected and the fibers were moved. Obviously, the PVA/MEG nanocomposite fiber-treated groups (0.1 and 0.3 wt % of MEG) almost have no unhealed wound areas compared to the other groups (see Figure 7b). To evaluate the microscopic appearances of local skin for the common surgical suture-treated group and the nanocomposite fiber with 0.3 wt % MEG-treated group on the 7 days, histological examination of the full-thickness wounds was performed (see Figure 7c,d). The number of inflammatory cells in the nanocomposite fiber with 0.3 wt % MEG-treated group was much less than that in the common surgical suture-treated group.

These results indicate that PVA/MEG nanocomposite fibers are efficacious for the healing of the wounds. It is not surprising that PVA/MEG nanocomposite fibers are better than the neat PVA fiber and common surgical suture for infectious wounds because of the outstanding antimicrobial properties and excellent mechanical properties. It is worth mentioning that the PVA/MEG nanocomposite fibers are smooth monofilament sutures. Compared with the rough surface of multibeam surgical sutures, the suture resistances of the PVA/MEG nanocomposite fibers are very small and will not cause secondary damage.

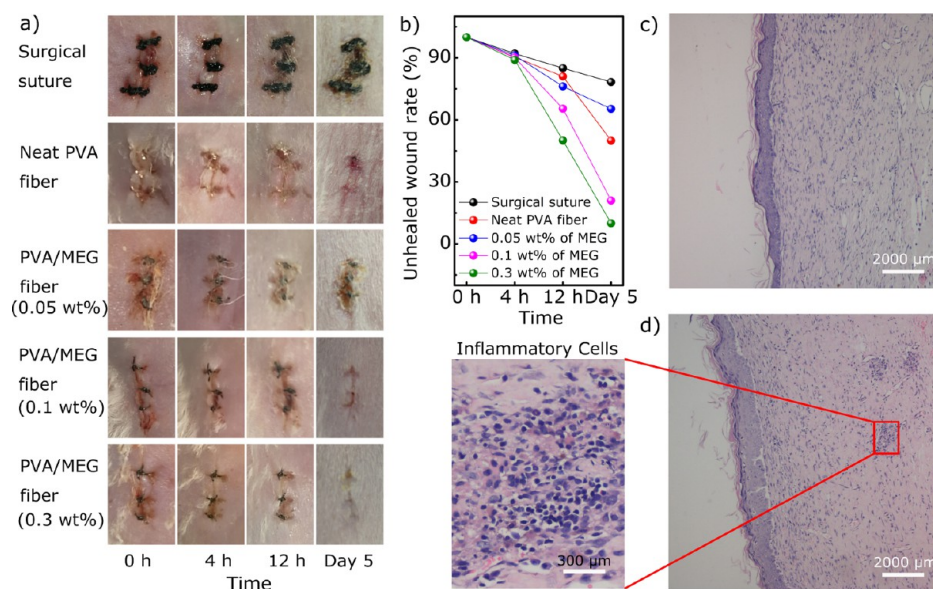


**Figure 7.** Wound healing evaluation of mice model. (a) Representative wounds at different times after surgery and (b) unhealed wound rate in five groups during 5 postoperative days. Histological examination of (c) nanocomposite fiber with 0.3 wt % of MEG-treated group and (d) common surgical suture-treated group.

### 3. CONCLUSIONS

In summary, we have obtained MEG with a high yield of 91% in viscous medium via a three-roll mill as a nanofiller for the PVA matrix. AFM, TEM, Raman spectra, and XPS have demonstrated that nonoxidized MEG has a complete structure and good electrical property. Furthermore, PVA/MEG nanocomposite fibers were prepared by gel spinning and a high ultimate tensile strength of 2.1 GPa was much higher than that of the neat PVA fibers of 0.75 GPa. The high strength is attributed to the uniform dispersion of MEG in PVA and noncovalent bonding with the polymer, which conducts the external forces on the polymer chains. On the basis of the good antibacterial properties and low cytotoxicity of PVA/MEG nanocomposite fibers, both the common surgical suture and the PVA/MEG nanocomposite fibers with three kinds of MEG loadings were valued on the mice model. The results showed that the wound healing cycle of the PVA/MEG nanocomposite fiber with 0.3 wt % of the MEG-treated group was the shortest. Therefore, the PVA/MEG nanocomposite fiber can be used as a promising new candidate for surgical sutures.

### 4. EXPERIMENTAL SECTION

**4.1. Materials.** Graphite powder with an average particle size of 25 μm and a purity of >99.9% was purchased from Sinopharm Chemical Reagent Co. Ltd (Shanghai, China); natural honey from Beijing Flowers Apiculture Technology Development Co. Ltd. (Beijing, China); and PVA ( $M_w \approx 74\,800$ ) from Kuraray Co. Ltd. (Japan). DMSO and ethanol were purchased from the Tianjin Guangfu Fine Chemical Research Institute (Tianjin, China). Cellulose acetate membranes were supplied by Xinya Purification Device Factory (Shanghai, China). Adult male Kunming mice, 6–8 weeks old, were obtained from the Animal Laboratory Center in Lanzhou University, and all the experimental designs were carried out in strict accordance with institutional guidelines of the Care and Use of Laboratory Animals. *S. aureus* (ATCC 25923), *E. coli* (ATCC 25922), and PBMC were obtained from the Lanzhou University School of Medicine. Surgical sutures were purchased from Yangzhou Yuan Kang Medical Devices Co., Ltd. (Yangzhou, China). All reagents are of chemical grade and were used as received without further purification.

**4.2. Preparation of Graphene.** First, the graphite powder (1 g) was added to honey (8 mL) and stirred at 200 rpm for 10 min by a mechanical stirrer. Then, the mixture was placed between the feed and the center rolls of a three-roll mill. In the three-roll machine rotation process, the high viscosity of the viscous medium will be evenly distributed in every roll, and the natural graphite was exfoliated for 3, 4, 4.5, and 5 h, respectively. Here, it is noted that, during the exfoliation process, the roller temperature and the humidity of the mixed material should be in a stable state. The productions with different peeling time were transferred to a beaker and washed three times with distilled water at 80 °C to remove the viscous medium and obtain the monolayer and multilayers of graphene. Finally, high-quality graphene can be separated from the mixture dispersion of exfoliated graphite by a centrifuge of 1000 rpm for 15 min, and then, the precipitate of unexfoliated graphite was removed.

**4.3. Fabrication of PVA/MEG Nanocomposite Fibers.** First, a certain amount of PVA and graphene at the expected ratio were slowly added into a mixed solution of DMSO and water at a volume ratio of 4:1 by shear mixing at 300 rpm and 80 °C for 1 h, and the solid content of the spinning solution was 0.16 g/mL. Next, the spinning solution was placed in a hot oven at 70 °C for 4 h to remove air bubbles and was spun into 75% ethanol solution at −10 °C by a syringe which was placed on a syringe pump at a rate of 1 mL/min. Then, the nascent fibers were taken out after 1 h and dried at room temperature for 24 h. Finally, the composite fibers were stretched 20 times on a hot plate at 180 °C.

**4.4. Characterization.** AFM was performed on an Asylum Research MFP-3D instrument in a tapping mode to investigate the heights and the lateral dimensions of the MEG sheets. The TEM images were recorded by using a FEI Tecnai F30 microscope. Raman spectra of graphene were obtained with a HORIBA Jobin Yvon LabRAM-HR800 microscope with a 532 nm argon-laser excitation. XPS was performed on the exfoliated graphene to study the chemical modification, and the XPS spectra were carried out on a Kratos AXIS Ultra DLD instrument with Al K $\alpha$  radiation at room temperature. For electrical testing, MEG was pressed into a circular thin flake with a diameter of 10 mm, and the conductivity was measured using the RTS-8 four-point probe tester. Tensile testing was performed through an Instron 3343 material testing machine at a loading rate of 2 mm/min with a gauge length of 10 mm. The morphological features of the PVA/MEG nanocomposite fibers were characterized by a Hitachi S-4800 SEM instrument with an accelerating voltage of 5 kV. Thermal gravimetric analysis for the samples was performed on a PerkinElmer

Diamond thermal analyzer from room temperature to 600 °C with a heating rate of 10 °C/min and with N<sub>2</sub> as the sample purge gas. Ultraviolet–visible spectra of PVA/MEG nanocomposite fibers were recorded via using a TU-1901/1900 spectrophotometer at a scanning wavelength between 200 and 1000 nm. On the basis of the recorded data in accordance with the Australia/New Zealand standard AC/NZS 439:1996, ultraviolet protection factor (UPF) was calculated as follows<sup>38</sup>

$$\text{UPF} = \frac{\int_{290}^{400} E_{\lambda} \times S_{\lambda} \times d\lambda}{\int_{290}^{400} E_{\lambda} \times S_{\lambda} \times T_{\lambda} \times d\lambda} \quad (4)$$

where  $E_{\lambda}$  is the relative erythral spectral effectiveness,  $S_{\lambda}$  is the solar UV spectral irradiance,  $T_{\lambda}$  is the spectral transmittance of the specimen,  $d\lambda$  is the wavelength increment (nm), and  $\lambda$  is the wavelength (nm).<sup>39</sup>

#### 4.5. Biological Tests of the PVA/MEG Nanocomposite Fibers.

In vitro antibacterial activity of PVA/MEG nanocomposite fibers was tested against the Gram-positive bacteria *S. aureus* (ATCC 25923) and the Gram-negative bacteria *E. coli* (ATCC 25922) in a suspension by using the viable cell-counting method. The fibers were mixed in phosphate-buffered (PB) solution, and a blank prepared with bacteria alone in PB solution was used as a control. Both of the two solutions were added to 2 mL PB suspension of microorganisms and incubated for 18 h at 37 °C with shaking. The samples were serially diluted and mixed with melted Luria–Bertani agar and poured into a sterile Petri dish. After incubation at 37 °C for 4 h, the numbers of bacterial colonies were counted and averaged from three replicate tests for each sample.

The toxicity of PVA/MEG nanocomposite fibers was measured after 4 h of exposure to these samples, and the survival of the bacteria was determined by measuring the growth curve by OD. After the exposure, the OD of every group in 200  $\mu$ L of fresh media was measured every half hour at 600 nm with a Synergy MX Microtiter plate reader. This process is repeated three times. Statistical analyses (two-sided *t*-test, 95% confidence interval) were implemented to identify whether the OD values of the samples with nanocomposite fibers were significantly different from the control.

The cytotoxicity of PVA/MEG nanocomposite fibers was investigated by a 3-(4,5-dimethylthiazol-2-yl)-2,5-diphenyl-tetrazolium bromide assay. PBMCs were seeded to a 96-well flat plate (Falcon, USA) and cultured in RPMI-1640 medium (Sigma-Aldrich, USA) supplemented with 10% heat-inactivated bovine serum and 1% streptomycin. The survival of PBMCs in the control sample and nanocomposite fibers was studied after 48 h. There is a linear relationship between the amount of the formazan compound produced by living cells and the number of living cells. All the results were calculated according to eq 5

$$\text{Live cells (\%)} = A_{\text{S}}/A_{\text{N}} \times 100\% \quad (5)$$

where  $A_{\text{S}}$  is the absorbance of samples and  $A_{\text{N}}$  is the absorbance of a negative control.

In vivo wound healing study was carried out by PVA/MEG nanocomposite fibers using an animal model. Adult male Kunming mice, 6–8 weeks old, were obtained from the Animal Laboratory Center in Lanzhou University. After the mice were anesthetized with an intraperitoneal injection of pentobarbital sodium (0.05 mg/g), the hair of the mice was removed and an open surgical wound of 1.5 cm in length was created on the dorsal skin by a scalpel, which was sterilized and exposed to air for 24 h. The wounds were sutured with common surgical sutures, neat PVA fiber, and PVA/MEG nanocomposite fibers, respectively. The postoperative mice were exposed to unsterilized air to create an ordinary wound healing environment.  $A_t$  postoperative hours 0, 4, 12, and 5 days later, the appearance of the wounds was photographed and the wound healing rate was calculated by the percentage of  $A_t/A_0$ , where  $A_t$  and  $A_0$  were the inflammation areas on the specified time and the time of operation, respectively. The wound with adjacent normal skin was excised at the seventh postoperative day

for counting inflammatory cells. Sections were stained with hematoxylin and eosin and counted using ImageJ 1.41 software.

## ■ ASSOCIATED CONTENT

### Supporting Information

The Supporting Information is available free of charge on the ACS Publications website at DOI: 10.1021/acsami.7b17835.

SEM of surfaces, thermal degradation behavior, and UV-blocking properties of PVA/MEG nanocomposite fibers (PDF)

## ■ AUTHOR INFORMATION

### Corresponding Author

\*E-mail: baiyx@lzu.edu.cn.

### ORCID

Yongxiao Bai: 0000-0001-5821-3015

### Notes

The authors declare no competing financial interest.

## ■ ACKNOWLEDGMENTS

We would like to thank the PetroChina project Foundation (kywx-17-006) and the National Natural Science Foundation of China (no. 50703017). We also acknowledge the support for the basic scientific research business expenses by the central university and Open Project of Key Laboratory for Magnetism and Magnetic Materials of the Ministry of Education, Lanzhou University.

## ■ REFERENCES

- Han, M. Y.; Özyilmaz, B.; Zhang, Y.; Kim, P. Energy band-gap engineering of graphene nanoribbons. *Phys. Rev. Lett.* **2007**, *98*, 206805.
- Munuera, J. M.; Paredes, J. I.; Enterría, M.; Pagán, A.; Villar-Rodil, S.; Pereira, M. F. R.; Martins, J. I.; Figueiredo, J. L.; Cenis, J. L.; Martínez-Alonso, A. Electrochemical Exfoliation of Graphite in Aqueous Sodium Halide Electrolytes toward Low Oxygen Content Graphene for Energy and Environmental Applications. *ACS Appl. Mater. Interfaces* **2017**, *9*, 24085–24099.
- Shen, H.; Zhang, L.; Liu, M.; Zhang, Z. Biomedical applications of graphene. *Theranostics* **2012**, *2*, 283.
- Inui, O.; Teramura, Y.; Iwata, H. Retention dynamics of amphiphilic polymers PEG-lipids and PVA-alkyl on the cell surface. *ACS Appl. Mater. Interfaces* **2010**, *2*, 1514–1520.
- Bin, Y.; Mine, M.; Koganemaru, A.; Jiang, X.; Matsuo, M. Morphology and mechanical and electrical properties of oriented PVA–VGCF and PVA–MWNT composites. *Polymer* **2006**, *47*, 1308–1317.
- Xu, X.; Uddin, A. J.; Aoki, K.; Gotoh, Y.; Saito, T.; Yumura, M. Fabrication of high strength PVA/SWCNT composite fibers by gel spinning. *Carbon* **2010**, *48*, 1977–1984.
- Geim, A. K.; Novoselov, K. S. The rise of graphene. *Nat. Mater.* **2007**, *6*, 183–191.
- Scholz, J.; Nocke, G.; Hollstein, F.; Weissbach, A. Investigations on fabrics coated with precious metals using the magnetron sputter technique with regard to their anti-microbial properties. *Surf. Coat. Technol.* **2005**, *192*, 252–256.
- Lee, C.; Wei, X.; Kysar, J. W.; Hone, J. Measurement of the elastic properties and intrinsic strength of monolayer graphene. *Science* **2008**, *321*, 385–388.
- Wang, C.; Li, Y.; Ding, G.; Xie, X.; Jiang, M. Preparation and characterization of graphene oxide/poly(vinyl alcohol) composite nanofibers via electrospinning. *J. Appl. Polym. Sci.* **2013**, *127*, 3026–3032.



- (11) Li, Y.; Sun, J.; Wang, J.; Qin, C.; Dai, L. Preparation of well-dispersed reduced graphene oxide and its mechanical reinforcement in polyvinyl alcohol fibre. *Polym. Int.* **2016**, *65*, 1054–1062.
- (12) Li, J.; Shao, L.; Zhou, X.; Wang, Y. Fabrication of high strength PVA/rGO composite fibers by gel spinning. *RSC Adv.* **2014**, *4*, 43612–43618.
- (13) Hu, X.; Ren, N.; Chao, Y.; Lan, H.; Yan, X.; Sha, Y.; Sha, X.; Bai, Y. Highly aligned graphene oxide/poly(vinyl alcohol) nanocomposite fibers with high-strength, antiultraviolet and antibacterial properties. *Composites, Part A* **2017**, *102*, 297–304.
- (14) Li, D.; Müller, M. B.; Gilje, S.; Kaner, R. B.; Wallace, G. G. Processable aqueous dispersions of graphene nanosheets. *Nat. Nanotechnol.* **2008**, *3*, 101–105.
- (15) Gao, W.; Li, J.; Yan, X.; Zhu, B.; Jia, J.; Huang, A.; Xie, K.; Bai, Y. Accordion-like graphene by a facile and green synthesis method reinforcing polyolefin nanocomposites. *RSC Adv.* **2017**, *7*, 31085–31092.
- (16) Hu, X.; Ouyang, S.; Mu, L.; An, J.; Zhou, Q. Effects of graphene oxide and oxidized carbon nanotubes on the cellular division, microstructure, uptake, oxidative stress, and metabolic profiles. *Environ. Sci. Technol.* **2015**, *49*, 10825–10833.
- (17) Hernandez, Y.; Nicolosi, V.; Lotya, M.; Blighe, F. M.; Sun, Z.; De, S.; McGovern, I. T.; Holland, B.; Byrne, M.; Gun'Ko, Y. K.; Boland, J. J.; Niraj, P.; Duesberg, G.; Krishnamurthy, S.; Goodhue, R.; Hutchison, J.; Scardaci, V.; Ferrari, A. C.; Coleman, J. N. High-yield production of graphene by liquid-phase exfoliation of graphite. *Nat. Nanotechnol.* **2008**, *3*, 563–568.
- (18) Coleman, J. N. Liquid exfoliation of defect-free graphene. *Acc. Chem. Res.* **2013**, *46*, 14–22.
- (19) Hernandez, Y.; Nicolosi, V.; Lotya, M.; Blighe, F. M.; Sun, Z.; De, S.; McGovern, I. T.; Holland, B.; Byrne, M.; Gun'Ko, Y. K. High-yield production of graphene by liquid-phase exfoliation of graphite. *Nat. Nanotechnol.* **2008**, *3*, 563–568.
- (20) Meyer, J. C.; Geim, A. K.; Katsnelson, M. I.; Novoselov, K. S.; Booth, T. J.; Roth, S. The structure of suspended graphene sheets. *Nature* **2007**, *446*, 60–63.
- (21) Zhou, Y.; Bao, Q.; Tang, L. A. L.; Zhong, Y.; Loh, K. P. Hydrothermal Dehydration for the “Green” Reduction of Exfoliated Graphene Oxide to Graphene and Demonstration of Tunable Optical Limiting Properties. *Chem. Mater.* **2009**, *21*, 2950–2956.
- (22) Graf, D.; Molitor, F.; Ensslin, K.; Stampfer, C.; Jungen, A.; Hierold, C.; Wirtz, L. Spatially resolved Raman spectroscopy of single- and few-layer graphene. *Nano Lett.* **2007**, *7*, 238–242.
- (23) Shin, H. J.; Kim, J.; Kim, S.; Kim, H.; Nguyen, V. L.; Lee, Y. H.; Lim, S. C.; Son, J.-H. Transient carrier cooling enhanced by grain boundaries in graphene monolayer. *ACS Appl. Mater. Interfaces* **2017**, *9*, 41026–41033.
- (24) Ferrari, A. C.; Meyer, J. C.; Scardaci, V.; Casiraghi, C.; Lazzeri, M.; Mauri, F.; Piscanec, S.; Jiang, D.; Novoselov, K. S.; Roth, S.; Geim, A. K. Raman spectrum of graphene and graphene layers. *Phys. Rev. Lett.* **2006**, *97*, 187401.
- (25) Arao, Y.; Mori, F.; Kubouchi, M. Efficient solvent systems for improving production of few-layer graphene in liquid phase exfoliation. *Carbon* **2017**, *118*, 18–24.
- (26) Xu, Y.; Bai, H.; Lu, G.; Li, C.; Shi, G. Flexible graphene films via the filtration of water-soluble noncovalent functionalized graphene sheets. *J. Am. Chem. Soc.* **2008**, *130*, 5856–5857.
- (27) Paton, K. R.; Varrla, E.; Backes, C.; Smith, R. J.; Khan, U.; O'Neill, A.; Boland, C.; Lotya, M.; Istrate, O. M.; King, P. Scalable production of large quantities of defect-free few-layer graphene by shear exfoliation in liquids. *Nat. Mater.* **2014**, *13*, 624–630.
- (28) Wang, Y.; Tong, X.; Guo, X.; Wang, Y.; Jin, G.; Guo, X. Large scale production of highly-qualified graphene by ultrasonic exfoliation of expanded graphite under the promotion of (NH<sub>4</sub>)<sub>2</sub>CO<sub>3</sub> decomposition. *Nanotechnology* **2013**, *24*, 475602.
- (29) Khan, U.; O'Neill, A.; Lotya, M.; De, S.; Coleman, J. N. High-concentration solvent exfoliation of graphene. *Small* **2010**, *6*, 864–871.
- (30) Peukert, W.; Schwarzer, H.-C.; Stenger, F. Control of aggregation in production and handling of nanoparticles. *Chem. Eng. Process. Process Intensif.* **2005**, *44*, 245–252.
- (31) Liu, X.; Zheng, M.; Xiao, K.; Xiao, Y.; He, C.; Dong, H.; Lei, B.; Liu, Y. Simple, green and high-yield production of single- or few-layer graphene by hydrothermal exfoliation of graphite. *Nanoscale* **2014**, *6*, 4598–4603.
- (32) Damm, C.; Nacken, T. J.; Peukert, W. Quantitative evaluation of delamination of graphite by wet media milling. *Carbon* **2015**, *81*, 284–294.
- (33) Zhao, W.; Fang, M.; Wu, F.; Wu, H.; Wang, L.; Chen, G. Preparation of graphene by exfoliation of graphite using wet ball milling. *J. Mater. Chem.* **2010**, *20*, 5817–5819.
- (34) Zhang, X.; Liu, T.; Sreekumar, T. V.; Kumar, S.; Hu, X.; Smith, K. Gel spinning of PVA/SWNT composite fiber. *Polymer* **2004**, *45*, 8801–8807.
- (35) Carpio, I. E. M.; Santos, C. M.; Wei, X.; Rodrigues, D. F. Toxicity of a polymer–graphene oxide composite against bacterial planktonic cells, biofilms, and mammalian cells. *Nanoscale* **2012**, *4*, 4746–4756.
- (36) Hu, W.; Peng, C.; Luo, W.; Lv, M.; Li, X.; Li, D.; Huang, Q.; Fan, C. Graphene-based antibacterial paper. *ACS Nano* **2010**, *4*, 4317–4323.
- (37) Chen, J.; Wang, X.; Han, H. A new function of graphene oxide emerges: inactivating phytopathogenic bacterium *Xanthomonas oryzae* pv. *Oryzae*. *J. Nanoparticle Res.* **2013**, *15*, 1658.
- (38) Tragoonwichian, S.; O'Rear, E. A.; Yanumet, N. Double coating via repeat admicellar polymerization for preparation of bifunctional cotton fabric: Ultraviolet protection and water repellence. *Colloids Surf., A* **2009**, *349*, 170–175.
- (39) Hu, X.; Tian, M.; Qu, L.; Zhu, S.; Han, G. Multifunctional cotton fabrics with graphene/polyurethane coatings with far-infrared emission, electrical conductivity, and ultraviolet-blocking properties. *Carbon* **2015**, *95*, 625–633.